


# Loss of BubR1 acetylation provokes replication stress and leads to complex chromosomal rearrangements

Jiho Park<sup>1</sup>, Song Y. Yeu<sup>1</sup>, Sangjin Paik<sup>1</sup>, Hyungmin Kim<sup>1</sup>, Si-Young Choi<sup>1</sup>, Junyeop Lee<sup>1</sup>, Jinho Jang<sup>2</sup>, Semin Lee<sup>2</sup>, Youngil Koh<sup>3</sup> and Hyunsook Lee<sup>1</sup> 

<sup>1</sup> Department of Biological Sciences & Institute of Molecular Biology and Genetics, Seoul National University, Korea

<sup>2</sup> Department of Bioengineering, School of Life Sciences, Ulsan National Institute of Science and Technology, Korea

<sup>3</sup> Department of Internal Medicine, Seoul National University Hospital, Korea

## Keywords

BubR1 acetylation; cancer; chromosomal instability; p53; replication stress

## Correspondence

H. Lee, Department of Biological Sciences & Institute of Molecular Biology and Genetics, Seoul National University, 1 Gwanak-Ro, Gwanak-Gu, Seoul 08832, Korea

Tel: +82 2 886 4339

E-mail: HL212@snu.ac.kr

(Received 26 November 2020, revised 25 March 2021, accepted 4 May 2021)

doi:10.1111/febs.15912

Accurate chromosomal segregation during mitosis is regulated by the spindle assembly checkpoint (SAC). SAC failure results in aneuploidy, a hallmark of cancer. However, many studies have suggested that aneuploidy alone is not oncogenic. We have reported that BubR1 acetylation deficiency in mice (*K243R/+*) caused spontaneous tumorigenesis via weakened SAC signaling and unstable chromosome-spindle attachment, resulting in massive chromosomal mis-segregation. In addition to aneuploidy, cells derived from *K243R/+* mice exhibited moderate genetic instability and chromosomal translocation. Here, we investigated how the loss of BubR1 acetylation led to genetic instability and chromosomal rearrangement. To rescue all chromosomal abnormalities generated by the loss of BubR1 acetylation during development, *K243R/+* mice were crossed with *p53*-deficient mice. Genome-wide sequencing and spectral karyotyping of tumors derived from these double-mutant mice revealed that BubR1 acetylation deficiency was associated with complex chromosomal rearrangements, including Robertsonian-like whole-arm translocations. By analyzing the telomeres and centromeres in metaphase chromosome spreads, we found that BubR1 acetylation deficiency increased the collapse of stalled replication forks, commonly referred to as replication stress, and led to DNA damage and chromosomal rearrangements. BubR1 mutations that are critical in interacting with PCAF acetyltransferase and acetylating K250, L249F and A251P, were found from human cancers. Furthermore, a subset of human cancer cells exhibiting whole-arm translocation also displayed defects in BubR1 acetylation, supporting that defects in BubR1 acetylation in mitosis contributes to tumorigenesis. Collectively, loss of BubR1 acetylation provokes replication stress, particularly at the telomeres, leading to genetic instability and chromosomal rearrangement.

## Abbreviations

APC/C, anaphase-promoting complex; ATCC, American Type Culture Collection; BubR1, Bub1-related protein 1; CIN, chromosomal instability; CldU, chlorodeoxyuridine; D box, destruction box; DMEM, Dulbecco's modified Eagle medium; DSMZ, Deutsche Sammlung von Mikroorganismen und Zellkulturen; EDTA, ethylenediaminetetraacetic acid; EdU, 5-ethynyl-2'-deoxyuridine; FISH, fluorescence *in situ* hybridization; H&E, hematoxylin and eosin; HDAC, histone deacetylase; IdU, iododeoxyuridine; MCC, mitotic checkpoint complex; MEF, mouse embryonic fibroblast; PCAF, P300/CBP-associated factor; PMSCS, premature sister chromatid separation; SAC, spindle assembly checkpoint; SCNA, somatic copy number alteration; SNUH, Seoul National University Hospital; SNV, single-nucleotide variation; SV, structural variation; TCGA, The Cancer Genome Atlas; T-loops, telomere loops.

## Introduction

Aneuploidy is the hallmark of cancer. Dysregulated chromosomal segregation during mitosis results in aneuploidy or death. Therefore, the loss or mutation of the genes involved in spindle assembly checkpoint (SAC) signaling has been suspected to cause aneuploidy. However, analyses using genetically engineered mice have revealed that aneuploidy itself is not oncogenic, but contributes to tumorigenesis only when combined with genotoxic stress [1].

BubR1 is a core component of SAC, which is part of the mitotic checkpoint complex (MCC) [2–4]. Homozygous deletion of *BubR1* in mice is embryonically lethal, whereas heterozygous deletion results in megakaryopoiesis and aneuploidy without any signs of spontaneous tumorigenesis [5]. Moreover, studies of hypomorphic *BubR1* alleles have suggested that decrease in BubR1 protein is associated with premature aging [6].

BubR1 is exclusively acetylated at lysine 250 (K250) during mitosis. BubR1 acetylation inhibits the activity of anaphase-promoting complex (APC/C) in prometaphase [7], and BubR1 deacetylation is a cue to MCC disassembly, leading to SAC silencing [8]. Importantly, BubR1 K250 residues are located adjacent to the degrons, the ABBA motif, KEN box, and D box [4,9]. We have hypothesized that BubR1 acetylation/deacetylation serves as a molecular switch for APC/C regulation [7]. Moreover, the tumor suppressor BRCA2 serves as a platform for BubR1 acetylation that it acts as a scaffold and mediates the binding between acetyltransferase P300/CBP-associated factor (PCAF) and BubR1. Consequently, BRCA2-deficient cells lack BubR1 acetylation at K250 [10]. Consistently, transgenic mice engineered to inhibit BRCA2 and BubR1 association develop tumors [10]. These results suggest that dysregulation of BubR1 acetylation can lead to spontaneous tumorigenesis, without interference of the regulatory role of BRCA2 in DNA repair [10].

Similarly, mice heterozygous for BubR1 acetylation at lysine 243 (*K243R/+*), which corresponds to K250 in humans, spontaneously develop tumors approximately 12 months after birth without apparent signs of premature aging [11]. Furthermore, study in *K243R/+* mice revealed that BubR1 K250 acetylation has the dual role of maintaining the MCC during checkpoint signaling and stabilizing chromosome-spindle attachment for chromosomal congression [11].

Chromosomes from *K243R/+* mouse embryonic fibroblasts (MEFs) display near-diploid aneuploidy. Premature sister chromatid separation (PMSCS), interchromosomal translocation, and an increased number

of micronuclei, which occur due to error correction failure during chromosome-spindle attachment, have also been increased in these MEFs [11]. Furthermore, *p53* cDNA analysis in primary tumors has revealed that missense mutations are induced as a result of BubR1 acetylation deficiency. Based on these results, we hypothesized that the genetic instability and chromosomal structure aberrations may be the underlying mechanism leading to tumorigenesis in the *K243R/+* mice.

To test the hypothesis, *K243R/+* mice were intercrossed to *p53*-null mice to unmask all chromosomal aberrations and mutations that would otherwise have been lost during embryogenesis in *K243R/+* mice. The breeding scheme was physiological as *p53* mutations were frequently found in tumors of *K243R/+* mice [11]. We were also interested to see whether chromothripsis, one-time chromosomal crisis and cis-rearrangement of chromosomes [12,13], could be found in tumors, as micronuclei were suggested source for chromothripsis [14], which were abundant in *K243R/+* cells while proliferation [11,15].

Here, we show that loss of BubR1 acetylation in mitosis induces replication stress and subsequent DNA damage, ultimately leading to complex chromosomal structure instability, including inter- and intrachromosomal rearrangements and Robertsonian-like whole-arm translocations. These features are also found in a subset of human cancers, including multiple myeloma. These data suggest that BubR1 acetylation deficiency may be involved in the tumorigenesis of cancers manifesting complex karyotypes.

## Results

### Loss of *p53* accelerates tumorigenesis with changes in tumor spectrum of *K243R/+* mice

Previously, we observed a small fraction of chromosomal translocation and missense mutations, along with aneuploidy, in primary MEFs derived from BubR1 acetylation-deficient (*K243R/+*) mice [11]. Because aneuploidy alone is not oncogenic and the outcome of aneuploidy in proliferating cells is complicated [1,16,17], we reasoned that the chromosomal structure aberrations and genetic instability may be the cause of tumorigenesis in the *K243R/+* mice. Aneuploidy would have exacerbated the situation [11].

To better understand tumorigenesis in the *K243R/+* mice, the mice were crossed with *p53*-null mice to unmask most of genetic and chromosomal aberrations. Wild-type (WT), *K243R/+*, *p53*<sup>−/−</sup>, and *K243R/+*; *p53*<sup>−/−</sup> compound mice were monitored up to

80 weeks from birth. Consistent with the previous report [11], 46% of *K243R/+* mice ( $n = 41$ ) developed spontaneous tumors within 12 months. All of the *K243R/+;p53-/-* mice ( $n = 33$ , 100%) and the *p53-/-* mice ( $n = 14$ , 100%) developed tumors: *K243R/+;p53-/-* mice exhibited a substantially shorter median tumor-free survival time of approximately 24 weeks compared with approximately 65 weeks in the *K243R/+* mice. The *p53-/-* mice had a tumor-free survival time similar to that of the *K243R/+;p53-/-* mice (Fig. 1A).

Interestingly, the tumor spectrum of the *K243R/+;p53-/-* mice slightly differed from that of the *K243R/+* mice. Tumors from the *K243R/+* mice were mostly of mesenchymal origin, including lymphomas, sarcomas, and hepatocellular carcinomas [11], and were not restricted to a specific type of tissue. However, an interesting change in the tumor spectrum was observed when the *K243R/+* mice were crossed with *p53-/-* mice. It has been well established that *p53-/-* mice develop mostly thymic lymphomas and some sarcomas [18,19]. As expected, all of the *p53-/-* mice developed tumors with our breeding scheme (70% thymic lymphomas [ $n = 7$ ] and 30% sarcomas [ $n = 3$ ]). Tumors from the *K243R/+;p53-/-* mice followed the same pattern as those of the *p53-/-* mice, but with a slight shift (58% nonlymphoid sarcomas [ $n = 11$ ] and 42% thymic lymphomas [ $n = 8$ ]) (Fig. 1B). Representative photographs of thymic lymphoma and spindle cell sarcomas from the *K243R/+;p53-/-* mice are shown in Fig. 1C.

### Loss of BubR1 acetylation induces replication stress

We previously identified near-diploid aneuploidy and PMSCS as hallmarks of *K243R/+* mice, along with premature chromosomal segregation and micronuclei [11]. Additionally, numerous studies have reported tumorigenesis in *p53*-deficient mice to be accompanied by polyploidy and aneuploidy [20]. Indeed, our analysis corroborated these findings because the *p53-/-* MEFs exhibited a high incidence of aneuploidy and polyploidy (Fig. 2A, *p53-/-*). The *K243R/+* MEFs displayed a high frequency of aneuploidy, but the incidence of polyploidy was lower compared with the *p53-/-* MEFs (Fig. 2A, *K243R/+*). However, the *K243R/+;p53-/-* MEFs exhibited even more perturbed cell chromosome numbers, including some cells with more than 80 chromosomes (Fig. 2A, *K243R/+;p53-/-*).

More than 20% of the *K243R/+* MEFs exhibited PMSCS, occurring from premature activation of the

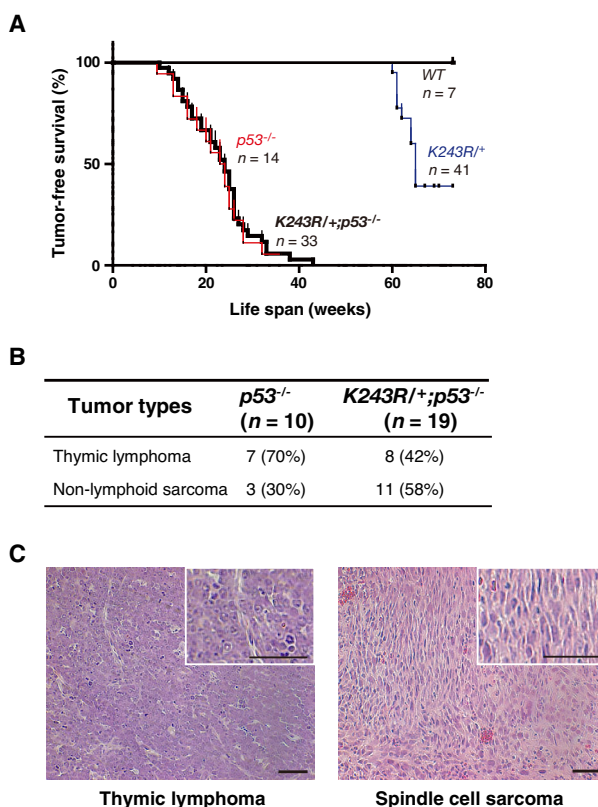


**Fig. 1.** Crossing with *p53*-deficient (*p53-/-*) mice leads to accelerated tumorigenesis and tumor spectrum changes in the acetylation-deficient BubR1 (*K243R/+*) mice. (A) Tumor-free survival was analyzed in wild-type (WT), *K243R/+*, *p53-/-*, and *K243R/+;p53-/-* mice (log-rank test). The median tumor-free survival time was determined (*K243R/+* vs. *K243R/+;p53-/-*,  $P < 0.0001$ ; *p53-/-* vs. *K243R/+;p53-/-*,  $P = 0.8282$ ; log-rank test). Tumor incidence was assessed by the Kaplan-Meier method. (B) The tumor spectrums of the *p53-/-* and *K243R/+;p53-/-* mice were determined. The *p53-/-* mice ( $n = 10$ ) exhibited malignant tumor development (70% thymic lymphomas,  $n = 7$ ; 30% nonlymphoid sarcomas,  $n = 3$ ). The *K243R/+;p53-/-* mice ( $n = 19$ ) exhibited thymic lymphoma (42%,  $n = 8$ ) and nonlymphoid sarcoma (58%,  $n = 11$ ). Lymphomas and nonlymphoid sarcomas were disseminated to multiple sites, including the thymus, legs, back, and bones. (C) Tumor sections from the *K243R/+;p53-/-* mice were stained with hematoxylin and eosin. Inset, enlarged image. Scale bar, 50  $\mu$ m.

APC/C without satisfying SAC. Approximately 10% of the *p53*-deficient MEFs displayed PMSCS. However, the incidence of PMSCS in the *K243R/+;p53-/-* MEFs was similar to that of the *K243R/+* MEFs (Fig. 2B).

Sequencing of *p53* cDNA from primary tumors derived from the *K243R/+* mice revealed that the majority of the tumors harbored the same missense

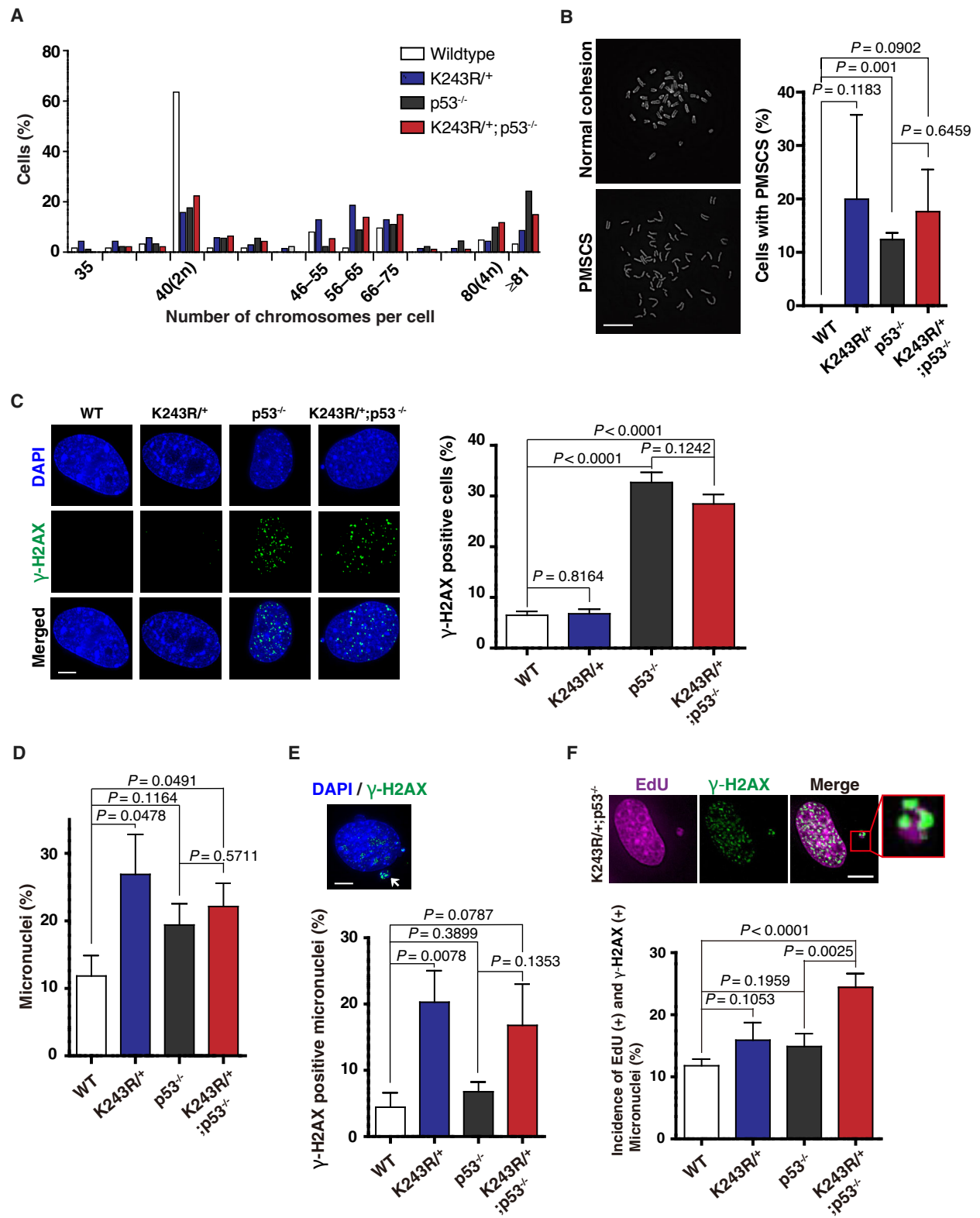


**Fig. 2.** Comparative analysis reveals chromosome and DNA damage in primary mouse embryonic fibroblasts. (A) The percentages of mouse embryonic fibroblasts (MEFs) with the indicated numbers of chromosomes were calculated. Fifty cells were analyzed from three independent experiments. In total, approximately 2000–2500 chromosomes were counted from each group. (B) Representative images of control (normal cohesion) and PMSCS are shown (left). Premature sister chromatid separation (PMSCS) was quantified in primary MEFs. Cells with more than five instances of PMSC were scored as positive (right). Twenty chromosome spreads from each of the indicated groups were scored in three independent experiments (mean  $\pm$  SEM;  $n = 60$ ). Scale bar, 10  $\mu$ m. *P*-values were determined by Student's *t*-test. (C) Representative images of immunofluorescence using the anti- $\gamma$ -H2AX antibody with DAPI counterstaining are shown. Scale bar, 5  $\mu$ m (left). Cells with  $\gamma$ -H2AX foci were quantified (right). Over 100 cells were scored in four independent experiments (mean  $\pm$  SEM). *P*-values were determined by Student's *t*-test. (D) The micronuclei in the mice were quantified. Two hundred cells were analyzed in four independent experiments (mean  $\pm$  SEM). (E) The  $\gamma$ -H2AX-positive micronuclei were quantified (right). Two hundred cells from each group were analyzed in four independent experiments (mean  $\pm$  SEM). A representative image of the  $\gamma$ -H2AX-positive micronuclei was acquired. Scale bar, 5  $\mu$ m. (F) Mouse embryonic fibroblasts (MEFs) from wild-type, *K243R/+*, *p53-/-*, and *K243R/+;p53-/-* mice were cultured with 10  $\mu$ M EdU for 12 h. The cells were then harvested and fixed with 4% paraformaldehyde. Incorporated EdU was visualized by cycloaddition reaction, and DNA was counterstained with DAPI. DNA damage was detected by immunostaining with an anti- $\gamma$ -H2AX antibody (upper panel). The EdU- and  $\gamma$ -H2AX-positive micronuclei were quantified (lower panel). More than 200 cells from each group were scored in three independent experiments. *P*-values were obtained from Student's *t*-test. Scale bar, 5  $\mu$ m.

*p53* mutations as those found in human cancers [11]. This result suggested that genetic instability was somehow triggered by the loss of BubR1 acetylation.

To unveil the basis of genetic instability after the loss of BubR1 acetylation, we investigated if the loss of BubR1 acetylation caused DNA damage. Immunofluorescence assay using an antibody against  $\gamma$ -H2AX revealed that the level of nuclear DNA damage in the *K243R/+* MEFs was comparable to that of the WT MEFs during interphase, which was consistent with our previous findings [11] (Fig. 2C, WT and *K243R/+*). In contrast, nuclear DNA damage was markedly increased in the *K243R/+;p53-/-* MEFs as well as the *p53-/-* MEFs (Fig. 2C, *p53-/-* and *K243R/+;p53-/-*).

Next, we investigated whether the micronuclei, which result from chromosomal mis-segregation [12], were the source of genotoxic insult in the *K243R/+* MEFs. Micronuclei were significantly increased upon loss of BubR1 acetylation. Micronuclei were found in *p53-/-* MEFs as well, but the effect was not as profound (Fig. 2D). To assess the damage of DNA in micronuclei, MEFs were immunostained with the anti- $\gamma$ -H2AX antibody and  $\gamma$ -H2AX-positive micronuclei were quantified. The results were considerably different from the nuclear DNA damage, because the number of  $\gamma$ -H2AX-positive micronuclei markedly increased in both the *K243R/+* and *K243R/+;p53-/-* MEFs, but less in the *p53-/-* MEFs (Fig. 2E).

Mouse embryonic fibroblasts were then pulsed with 5-ethynyl-2'-deoxyuridine (EdU) for 12 h to evaluate DNA synthesis while proliferation. Immunostaining with antibodies to anti- $\gamma$ -H2AX- and anti-EdU antibodies was performed and the double-positive

micronuclei scored. Micronuclei in MEFs doubly positive for EdU and  $\gamma$ -H2AX indicates that DNA synthesis and damage occurred in micronuclei, referring to replication stress. When more than 200 cells were scored from each group, it showed that DNA replication and damage in micronuclei were slightly higher in *p53-/-* and *K243R/+* MEFs, and  $\sim 2.5$ -fold higher in *K243R/+;p53-/-* MEFs (Fig. 2F).

Aneuploidy has been shown to cause an imbalance in replication machinery, resulting in replication stress. Because chromosomal mis-segregation with a shortened mitotic timing led to aneuploidy (numerical CIN) with little cell death in *K243R/+* MEFs, we investigated whether loss of BubR1 acetylation promoted replication stress in nuclear DNA. DNA fiber assay was performed to assess the fidelity of replication progression, as described [21,22]. Primary MEFs were first pulsed with iododeoxyuridine (IdU) for 20 min, washed, and then pulsed with chlorodeoxyuridine (CldU) for 60 min. Cells were collected, streaked on silane-coated slides, lysed, and DNA fiber was stretched. DNA-coated slides were fixed, and IdU and CldU were detected with red and green fluorescent-coupled antibodies, respectively (Fig. 3A).

Replication progression was quantified by the fiber track length (IdU + CldU), and the CldU/IdU ratio in the fiber could also be measured. Loss of BubR1 acetylation resulted in shortened replication fiber in the *K243R/+* and *K243R/+;p53-/-* MEFs. This effect was also observed in the *p53-/-* MEFs with lesser impact (Fig. 3A, *p53-/-* in graph). Note that the replication impediment is more profound in *K243R/+;p53-/-* MEFs (Fig. 3A, graph). By comparing the CldU/IdU ratios, we corroborated that *K243R/+* and



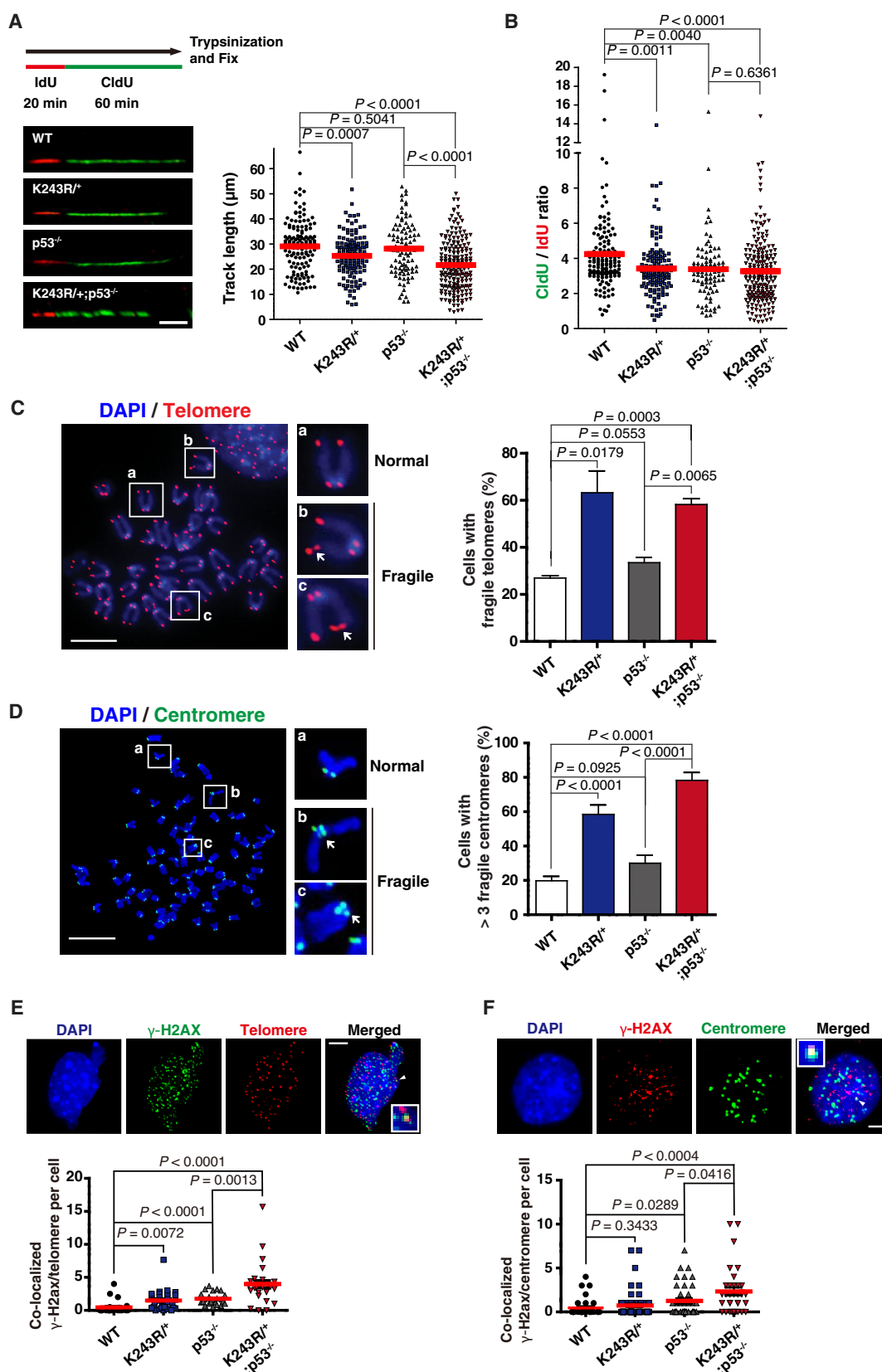


**Fig. 3.** Replication stress in nuclear DNA of *K243R/+;p53-/-* MEFs. (A) Ongoing replication was assessed by DNA fiber assay (left). Cells were first pulsed with IdU for 20 min, followed by incubation with CldU for 60 min. Cells were trypsinized, fixed, and then analyzed under the microscope. Representative images of the IdU (red) + CldU (green) track lengths are shown. The IdU + CldU track lengths were measured (right). Discontinuous fibers were observed in the *K243R/+;p53-/-* mouse embryonic fibroblasts (MEFs). Scale bar, 5  $\mu$ m (left). Each dot in the graph represents the track length of one fiber (right). (B) The distribution of the CldU/IdU ratios in the DNA fiber assay is shown. At least 90 well-isolated DNA fibers were scored for IdU + CldU-labeled tracks, and the IdU/CldU ratios were measured. The results are from two independent experiments. (C) Replication stress was revealed by telomere fluorescence *in situ* hybridization (FISH) (red) in metaphase chromosome spreads. Enlarged images of the insets are shown. The arrows indicate the fragile telomeres (gapped telomere FISH signals), representing discontinuous replication (left). The cells with fragile telomeres in each group were quantified (right). The bars represent the results of three independent experiments (mean  $\pm$  SEM). Scale bar, 5  $\mu$ m. (D) Centromere integrity was examined by centromere FISH. Enlarged images of the insets are shown. The arrows indicate the fragile centromeres (left). The cells with fragile centromeres were quantified (right). Twenty chromosome spreads were scored in three independent experiments (mean  $\pm$  SEM). Scale bar, 10  $\mu$ m. (E) Mouse embryonic fibroblasts (MEFs) from wild-type, *K243R/+*, *p53-/-*, and *K243R/+;p53-/-* mice were subjected to fluorescence *in situ* hybridization (FISH) analysis using a Cy-3-labeled telomere probe (red) and were immunostained with an anti- $\gamma$ -H2AX antibody (green). Cells were also counterstained with DAPI (blue). Telomere-colocalized  $\gamma$ -H2AX was quantified per cell (lower panel). At least 20 randomly selected cells from each group were analyzed in three independent experiments. Scale bar, 5  $\mu$ m. (F) MEFs from wild-type, *K243R/+*, *p53-/-*, and *K243R/+;p53-/-* mice were subjected to FISH analysis using a FAM-labeled centromere probe (green) and were immunostained with an anti- $\gamma$ -H2AX antibody (red, upper panel). Centromere-colocalized  $\gamma$ -H2AX was measured (lower panel). At least 30 randomly selected cells for each genotype were analyzed. Scale bar, 5  $\mu$ m.

*p53-/-* MEFs both displayed breakdown of stalled replication forks (Fig. 3B). Intriguingly, the majority of the DNA fibers analyzed in the *K243R/+;p53-/-* MEFs were gapped and discontinuous (Fig. 3A, *K243R/+;p53-/-*), indicating significant problems in fork progression. Discontinuous replication indicates the destabilization of the stalled replication forks, referred to as fragility and replication stress [23]. These results indicated that the loss of BubR1 acetylation promoted replication stress in nuclear DNA.

Centromeres and telomeres have been identified as hard-to-replicate regions due to tandem repeat sequences that can impede replication fork progression. Therefore, we next investigated whether BubR1 acetylation deficiency induced telomere and/or centromere fragility. Telomere and centromere fluorescence *in situ* hybridization (FISH) was performed on metaphase chromosome spreads. FISH signals that were gapped or tailed, instead of forming punctate foci, were considered fragile (Fig. 3C,D, arrows in inset). The *p53-/-* MEFs exhibited a slight increase in centromere and telomere fragility, but it was not to a considerable level. In contrast, centromere and telomere fragility was dramatically increased in the *K243R/+* and *K243R/+;p53-/-* MEFs (Fig. 3C,D, graph).

The MEFs were next subjected to immunofluorescence assay using the anti- $\gamma$ -H2AX antibody coupled with telomere or centromere FISH. A slight increase in centromere and telomere damage was detected in the *K243R/+* and *p53-/-* MEFs in interphase (Fig. 3E,F). Notably, there was significant telomere damage in the *K243R/+;p53-/-* MEFs in interphase (Fig. 3E).

### Tumorigenesis due to loss of BubR1 acetylation involves massive inter- and intrachromosomal rearrangements

Errors in mitosis and the resulting micronuclei have been suggested to be the sources of chromothripsis [12,13], the one-off catastrophic chromosomal breakage and cis-rearrangement [14], found in many types of cancer [24], particularly in those with p53 loss [25]. Furthermore, telomere crisis has been shown to induce chromothripsis and kataegis, the cancer genome signature involving the base substitution of C>T and C>G near chromothripsis breakpoints [26]. Because tumorigenesis by the loss of BubR1 acetylation resulted from mitotic infidelity, and a marked increase in telomere fragility occurred in the *K243R/+* MEFs, we investigated whether chromothripsis and kataegis were present in tumors of the *K243R/+;p53-/-* mice.

Whole-genome next-generation sequencing was performed for cultured primary liver cancer cells from the *K243R/+* mice and sarcoma cells cultured from the *p53-/-* and *K243R/+;p53-/-* mice. Deep sequencing was performed at an average depth of approximately 41 $\times$  for the cancer cells, along with paired constitutional DNA from healthy liver tissue. The sequencing data were then analyzed for copy number changes using BIC-seq2 [27].

Using Meerkat followed by specific quality filtering [28], we found 11 predicted inter- and intrachromosomal breakpoints in the cultured sarcoma cells from the *p53-/-* mice (Fig. 4A, *p53-/-*). However, the intra- and interchromosomal breakpoints and rearrangements

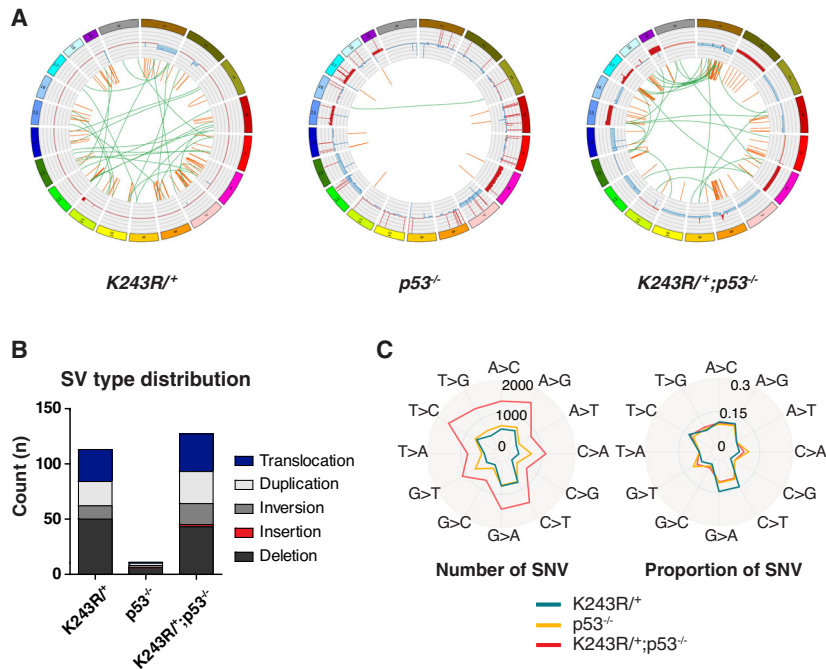


**Fig. 4.** Intra- and interchromosomal translocation by the loss of BubR1 acetylation. (A) Circos maps of whole-genome sequencing are shown, and chromosomes are depicted as individual colors. Data were from primary liver cancer cells from the *K243R/+* mice, cultured sarcoma cells from the *p53<sup>-/-</sup>* mice, and cultured sarcoma cells from the *K243R/+;p53<sup>-/-</sup>* mice. Copy numbers of the genomic region are plotted as gains (red) and losses (blue) as log<sub>2</sub> ratios. Chromosomal rearrangements are depicted on each side of the breakpoints, and intrachromosomal rearrangements (orange) and interchromosomal rearrangements (green) are located in the center of the circle. (B) Chromosomal structural variations (SVs) in the tumors of the *K243R/+*, *p53<sup>-/-</sup>*, and *K243R/+;p53<sup>-/-</sup>* mice were identified. The frequency of translocation, duplication, inversion, insertion, and deletion are depicted as bar graphs. (C) The spectrum of single-nucleotide variations (SNVs) from the tumor cells was evaluated. Total numbers (left) and the proportions of somatic SNVs (right) are shown.

were drastically increased in response to loss of BubR1 acetylation. We identified 113 breakpoints in the *K243R/+* primary liver cancer cells (Fig. 4A, *K243R/+*) and 127 breakpoints in the *K243R/+;p53<sup>-/-</sup>* sarcoma cells (Fig. 4A, *K243R/+;p53<sup>-/-</sup>*).

Oscillation between two copy number states has been identified as one of the characteristics of chromothripsis [29]. In our analysis, oscillation between two copy number states was hard to define; however, complex copy number variations were apparent (Fig. 4A). It was possible that chromothripsis was concealed in our analysis because of the various types of complex rearrangements. Chromosomal duplication, inversion, insertion, and deletion were also significantly induced by the loss of BubR1 acetylation (Fig. 4B). Altogether, these data suggested that loss of BubR1 acetylation resulted in chromosome shattering that led to complex structural variations, including intra- and interchromosomal translocation, rearrangements, and potentially chromothripsis.

Analysis of the genome-wide single-nucleotide variation (SNV) spectrum revealed the predominant mutation types. T > C, A > G, G > A, and C > T variations were the most common, followed by T > G and A > C (Fig. 4C). This spectrum was highly similar among the *K243R/+*, *p53<sup>-/-</sup>*, and *K243R/+;p53<sup>-/-</sup>* tumor cells. In total, 5140 SNVs were identified in the *K243R/+* tumor cells, 6801 were identified in the *p53<sup>-/-</sup>* cells, and 14 022 were identified in the *K243R/+;p53<sup>-/-</sup>* cells. (Fig. 4C, left). However, G > T and C > A mutations were relatively more common in the *p53<sup>-/-</sup>* cells, whereas T > C mutations occurred slightly more in the *K243R/+* tumor cells (Fig. 4C, right). Consistent with the uncertainty of chromothripsis breakpoints, kataegis was not verified in the tumors from the *K243R/+* or *K243R/+;p53<sup>-/-</sup>* mice. Nevertheless, these results suggested that loss of BubR1 acetylation induced genetic instability, which was reflected by random point mutations as well as chromosomal rearrangements.



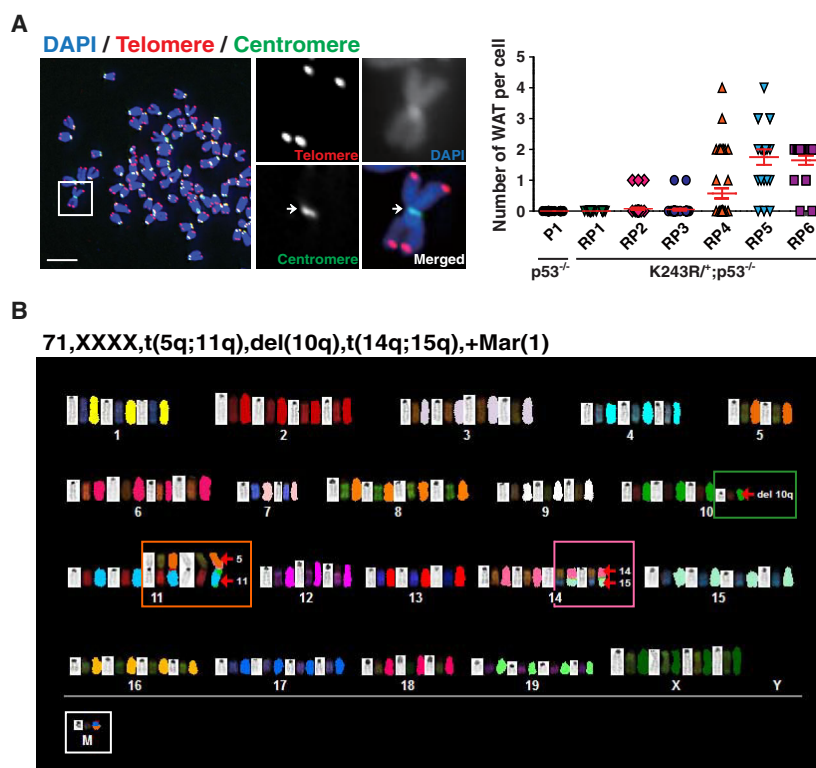


**Fig. 5.** Tumors from the *K243R/+; p53*<sup>-/-</sup> mice display Robertsonian-like whole-arm translocation. (A) Metaphase chromosomes of established sarcoma and lymphoma cells from the *K243R/+; p53*<sup>-/-</sup> mice were subjected to centromere and telomere FISH. Centromeres were detected by hybridization with a fluorescein-labeled probe (green), and telomeres were detected by a Cy3-labeled probe (red). Chromosomal DNA was counterstained with DAPI (blue). The arrow indicates a fused centromere without telomeres at the fusion point. Scale bar, 5  $\mu$ m (left). The number of whole-arm translocations was quantified for each cell. P1, *p53*-deficient sarcomas; RP1-6, tumors from the *K243R/+; p53*<sup>-/-</sup> mice (RP1-4, sarcomas; RP5 and RP6, lymphomas). All tumor cells were analyzed at early passages (below passage 10). Forty cells each were scored (mean  $\pm$  SEM,  $n = 40$ ) (right). (B) Representative spectral karyotyping of a sarcoma (RP4) from *K243R/+; p53*<sup>-/-</sup> mice is shown. Whole-arm translocation between chromosomes 5 and 11 (orange box), interchromosomal translocation between chromosomes 14 and 15 (pink box), deletion of chromosome 10 (green box), and a minute chromosome (white box, M) are displayed, and the karyotype of the examined tumor cell is indicated.

### Robertsonian-like whole-arm translocation as a signature of tumors from the *K243R/+; p53*<sup>-/-</sup> mice

Because telomere fragility was a significant feature of the *K243R/+* MEFs, we used centromere and telomere FISH on metaphase chromosome spreads to determine whether tumors from the *K243R/+; p53*<sup>-/-</sup> mice exhibited any further chromosomal aberrations related to telomere erosion. Strikingly, whole-arm translocation between the two chromosome short arms led to X-shaped chromosomes, rather than U-shaped telocentric mouse chromosomes, in *K243R/+; p53*<sup>-/-</sup> cells (Fig. 5A). Five out of six tumors from the *K243R/+; p53*<sup>-/-</sup> mice exhibited whole-arm translocation. Of these tumors, three (RP4, RP5, and RP6) displayed

more than two fusions per cell, whereas another two cells (RP2 and RP3) exhibited single fusion per cell (Fig. 5A, graph at right). We did not detect this Robertsonian-like whole-arm translocation in *p53*<sup>-/-</sup> cells (Fig. 5A, P1), consistent with the fact that it was never reported previously in tumors derived from *p53*<sup>-/-</sup> mice (Fig. 5A, right).

At the short arm of mouse chromosomes, the centromeres and telomeres are proximal to each other. At the fusion point, telomere signal was lost; however, the centromeres were intact (Fig. 5A, arrows in enlarged images). These results suggested an interesting hypothesis that telomere erosion induced end-to-end fusions, while centromere specification remained unperturbed in these fused chromosomes. Therefore, the X-shaped

**Table 1.** BubR1 mutations proximal to K250 and the status of acetylation.

BubR1 mutation	K250 acetylation in mitosis	p53 mutation	Cancer type	Sample ID	Study
P241A	O	–	Breast invasive lobular carcinoma	TCGA-D8-A73U-01	Breast Invasive Carcinoma (TCGA, Pan-Cancer Atlas)
P241T	O	–	Cutaneous melanoma	TCGA-FS-A1ZM-06	Skin Cutaneous Melanoma (TCGA, Pan-Cancer Atlas)
R244C	O	–	Cutaneous melanoma	TCGA-D3-A1Q6-06	Skin Cutaneous Melanoma (TCGA, Pan-Cancer Atlas)
		L111Q	Cutaneous melanoma	MEL-JWCI-WGS-25	Skin Cutaneous Melanoma (Broad, Cell 2012) [31]
R244S	O	K139fs*31	Lung adenocarcinoma	TCGA-05-4396-01	Lung Adenocarcinoma (TCGA, Pan-Cancer Atlas)
		-	Cutaneous melanoma	TCGA-BF-A1PZ-01	Lung Adenocarcinoma (TCGA, Pan-Cancer Atlas)
G246R	O	-	Cutaneous melanoma	TCGA-DA-A1I0-06	Skin Cutaneous Melanoma (TCGA, Pan-Cancer Atlas)
		-	Cutaneous melanoma	YUCLAT	Skin Cutaneous Melanoma (Yale, Nat Genet 2012) [33]
L249F	X	-	Skin cancer, nonmelanoma	5-PT055-T1	Basal Cell Carcinoma (UNIGE, Nat Genet 2016) [30]
A251P	X	V73Rfs*76	Renal clear cell carcinoma	TCGA-A3-3313-01	Kidney Renal Clear Cell Carcinoma (TCGA, Pan-Cancer Atlas)
N255Y	O	-	Rhabdomyosarcoma	RMS240	Rhabdomyosarcoma (NIH, Cancer Discov 2014) [34]
P261S	O	P278S, P278L	Cutaneous melanoma	Pt14	Metastatic Melanoma (UCLA, Cell 2016) [32]

The results here are based upon data generated by the TCGA Research Network: <https://www.cancer.gov/tcga>.

whole-arm translocated chromosomes may have been transmitted during cell division, similar to the Robertsonian translocation.

Spectral karyotyping corroborated the presence of whole-arm translocation in the *K243R/+;p53-/-* sarcoma cells (Fig. 5B, orange box). Interchromosomal rearrangements (Fig. 5B, pink box) and minute chromosomes (Fig. 5B, M, white box) were also observed, confirming that various structural chromosomal instabilities accompany tumorigenesis in response to the loss of BubR1 acetylation. Figure 5B shows the translocations between chromosomes 5 and 11, as well as chromosomes 14 and 15. However, analysis of other sets of spectral karyotyping revealed that the chromosomal fusion appeared random and was not restricted to specific mouse chromosomes, at least at this stage of culture (passage 10).

### Loss of BubR1 acetylation in human cancers

BubR1 acetylation deficiency in mice led to tumorigenesis through chromosomal mis-segregation, which was due to the combination of a weakened SAC and failure in the stabilization of chromosome-spindle attachment [11]. Extending our previous report, we showed

here that BubR1 acetylation deficiency promoted replication stress, resulting in genetic instability and various types of chromosomal structural aberrations during mouse tumorigenesis.

We next investigated whether BubR1 acetylation deficiency was found in human cancers. In the Cancer Genome Atlas (TCGA) database (cBioPortal), we did not find an exact K250 mutation in *BubR1*. However, we found nine mutations proximal to K250 of *BubR1* from the TCGA database using cBioPortal (Table 1) [30–34]. Therefore, we decided to assess these mutants for mitosis-specific K250 acetylation. The following nine mutants were evaluated: *BubR1* mutation at *P241A* identified in breast invasive lobular carcinoma; *P241T*, *R244C*, *G246R*, and *P261S* in melanoma; *R244S* in lung adenocarcinoma and melanoma; *L249F* in skin cancer (nonmelanoma); *A251P* in renal cell carcinoma; and *N255Y* in rhabdomyosarcoma [35,36] (Table 1). Mutant *BubR1* constructs tagged with Myc at the N terminus were generated by site-directed mutagenesis and were transfected into 293T cells. Two days after transfection, cells were treated with nocodazole to induce mitotic arrest. The cells were then subjected to immunoprecipitation using an anti-Myc antibody, followed by western blot analysis using the

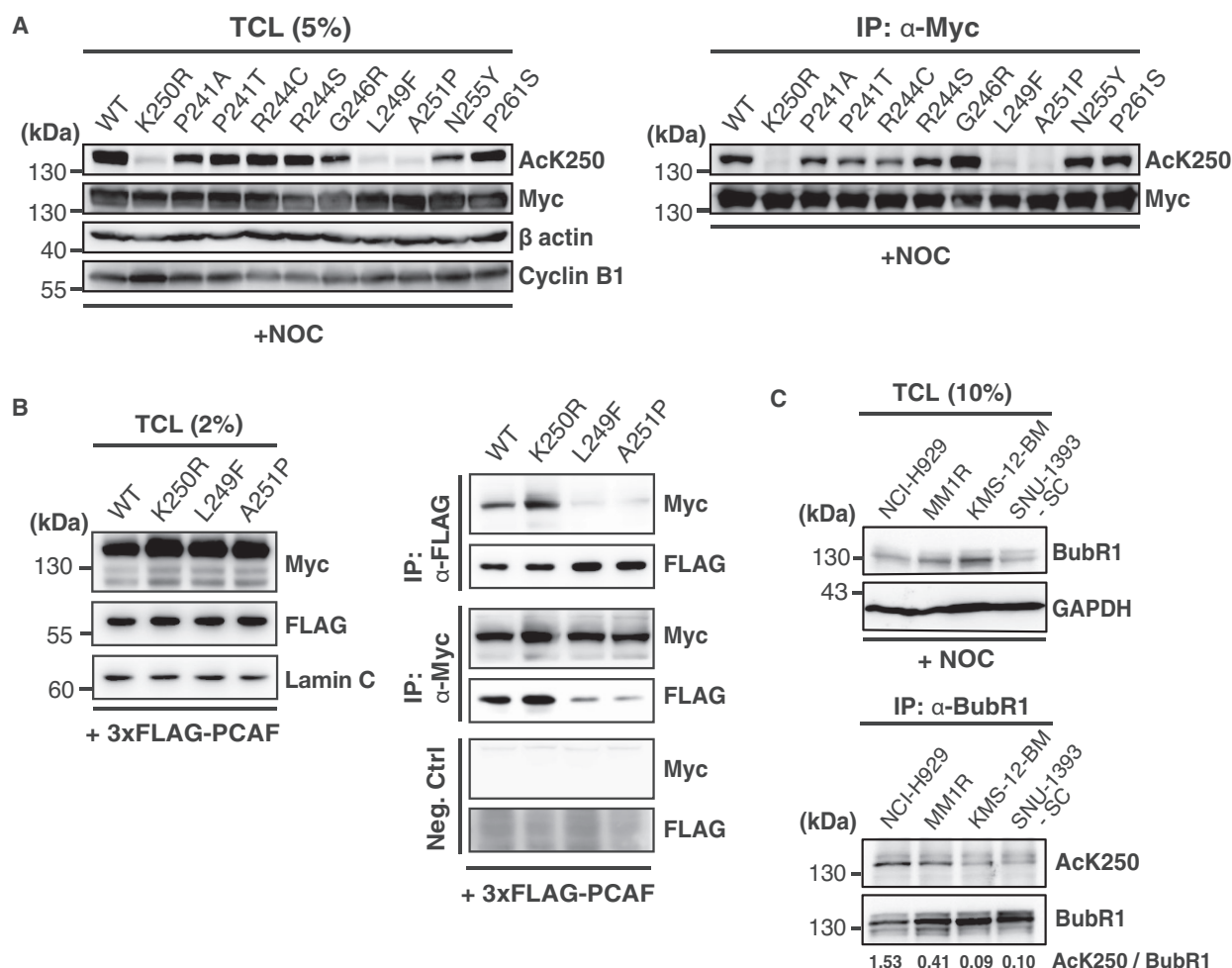


**Fig. 6.** BubR1 acetylation deficiency contributes to the pathogenesis of human malignant tumors. (A) Various BubR1 mutations near K250 acetylation sites were identified from The Cancer Genome Atlas (TCGA) database, and site-directed mutagenesis was performed to generate Myc-tagged BubR1 mutant constructs. The constructs were then transfected into HEK293T cells, followed by nocodazole treatment to induce mitotic arrest. The selected mutations were evaluated for mitosis-specific BubR1 acetylation by immunoprecipitation using an anti-Myc antibody, followed by western blot analysis using a monoclonal antibody against acetylated BubR1 (anti-AcK250). The same blot was reprobed with anti-Myc (9E10) antibody as a loading control. Ten percent of the total cell lysates (TCL) were subjected to western blot as a control. The K250R mutant was also used as a control. (B) Myc-tagged WT *BubR1*, K250R, L249F, and A251P-*BubR1* mutant constructs were cotransfected into HEK293T cells with plasmid encoding 3xFLAG-PCAF (352-832 amino acids), which contains HAT domain and bromodomain. Twenty-Four hours after transfection, cell lysates were subjected to co-immunoprecipitation with anti-FLAG (M2) antibody or anti-Myc (9E10) antibody, followed by western analysis with the antibodies indicated. To confirm the result, IP and WB were repeated in a reciprocal way. Two percent of total cell lysates (TCL) were subjected to western blot as a control. Mouse IgG was used as negative immunoprecipitation control. (C) Human multiple myeloma cell lines, NCI-H929, MM1R, KMS-12-BM, and SNU-1393-SC, were assessed for BubR1 acetylation during mitosis by immunoprecipitation and western blot using the anti-AcK250 monoclonal antibody. Cells were arrested in mitosis by nocodazole treatment. Ten percent of the TCL were subjected to western blot analysis. The numbers below indicate the AcK250/BubR1 ratio, as calculated by the band intensity, measured with the densitometer.

monoclonal anti-acetyl-K250 antibody [7,8]. Wild-type BubR1 (WT) and acetylation-deficient mutant *BubR1* (K250R) constructs were used as controls. The result showed that L249F and A251P mutants were completely defective in BubR1 acetylation comparable to the K250R control (Fig. 6A).

To unveil the molecular mechanism of how L249F and A251P mutants exhibit defects in BubR1 acetylation at K250, we asked if the mutation interfered with the interaction with acetyltransferase PCAF, as PCAF is the specific acetyltransferase that acetylates BubR1 at K250 in mitosis [7,10].

**Table 2.** Frequency of whole-arm translocation in hematopoietic malignancies from patients of Seoul National University Hospital (SNUH). Number of analyzed patients and the cases with whole-arm translocation (cases with whole-arm translocation) are shown.

Disease	Number of patients	Cases of whole-arm translocation (WAT)
Acute myeloid leukemia	730	15
Multiple myeloma	334	39
Acute lymphoblastic leukemia	219	2
Myelodysplastic neoplasms	158	13
Lymphoma	128	5
Diffuse large B-cell lymphoma	80	1
Chronic myeloid leukemia	79	1
Aplastic anemia	49	1
Chronic lymphocytic leukemia	23	1
Essential thrombocythemia	23	2
Idiopathic myelofibrosis	11	1
Monoclonal gammopathy of undetermined significance	2	1
Myelomatosis	1	1
Total	1837	83

FLAG-tagged PCAF-expressing construct and Myc-tagged BubR1 mutants were cotransfected into 293T cells and were subjected to Co-IP and WB, using anti-Myc or anti-FLAG antibodies, in a reciprocal way. The result showed that L249F and A251P were incapable of binding to PCAF, whereas wild-type or K250R did (Fig. 6B). In the protein interaction between PCAF and the target protein, it is known that the bromodomain of PCAF is most responsible. Notably, lysine recognition of bromodomain is dependent on amino acid residues at (K+/-1) or (K+/-2), just adjacent to acetyl-lysine in the target region [37]. The result that L249F and A251P mutants were devoid of K250 acetylation is consistent with the report: Point mutation at L249 or A251 interfered with the interaction with the bromodomain of PCAF and acetylate K250. In comparison, K250R had no problem interacting with PCAF: It only had lost the lysine for acetylation. The result speaks to the fact that BubR1 acetylation deficiency is pathogenic in human as well.

BubR1 K250 residues are located at the unstructured region near the degrons required for APC/C and/or Cdc20 recognition [3,4,9]. Because this region is

**Table 3.** List of multiple myeloma cell lines used in this study and its cytogenetic information.

Cell lines	Source	Accession Number	Cell types	Whole-arm-translocation	Cytogenetics	References
NCI-H929	ATCC	CRL-9068	Multiple myeloma	-	Near tetraploid, Most copies of chromosome 8 have the 8q+ abnormality	[41]
	DSMZ	ACC 163			Human hypodiploid karyotype with 16% polyploidy - 45(43-46)X, -X, +8, -10, -13, +mar, dup(1)(q11q25), del(1)(p11p25), del(6)(q25), der(8)t(8;?)(q23;?)x2, del(9)(p13), del(12)(p12)	
MM.1R	ATCC	CRL-2975	Multiple myeloma	-	t(12;14)(q24.3;q32.3), t(14;16)(q32;q23)	[42]
KMS-12-BM	DSMZ	ACC 551	Multiple myeloma	der(1;8)(q10;q10), der(5;17)(p10;q10)	Human flat-moded hypertriploid karyotype with 3% polyploidy - 69-79XX, -X, +1, +1, -4, +5, +6, +8, +9, -10, +13, +14, -15, -16, +17, -18, +19, +20, +21, -22, +4-5mar, der(1)t(1;4)(q11;q32), del(1)(p21)x2, der(1;8)(q10;q10)x2, add(4)(q32)x1-2, der(5;17)(p10;q10)x2, add(6)(q2?5), der(9)add(9)(p24)t(9;11)(q34;q13), der(9)t(9;11)(q34;q13), der(11)t(11;14)(q13;q32)x2-3, idic(?;13)(?;q32-33)x2, der(14)t(11;14)(q13;q32), der(17)t(11;17)(q21.2;q22)t(11;14)(q13;q32)x2, add(19)(q13), add(19)(q13)—related to published karyotype—carries semicryptic t(11;14) with IGH-CCND1 rearrangement	[39]
SNU-1393-SC	-	-	Multiple myeloma	der(1; 8) (q10; q10), der(1; 19) (q10; p10)	Karyotype: 74-76, X, der(X)t(X; 1)(q28; q21), add(1)(q11), der(1; 8) (q10; q10), der(1; 19)(q10; p10), +der(1; 19), add(3)(p26), -4, -5, +6, +add(7)(p15), der(9)t(9; 11)(q34; q13), +der(9)add(9)(p22)t(9; 11) (q34; q13), -10, -11, -11, -11, +add(12)(p13), -13, der(14)t(11; 14) (q13; q32), add(15)(q26), -16, -16, -17, -17, add(17)(p11.2), +18, +20, -22, -22, +14-16mar[cp10]	[40]

crucial for modulating APC/C activity, and the structure of the APC/C-MCC is complex, it will be interesting to see how L249F or A251P mutation alters the usage of the degrons, APC/C-MCC structure, compared to acetylated K250-BubR1.

Next, we determined whether whole-arm translocation was a feature associated with BubR1 acetylation deficiency in human cancer. Whole-arm translocation in human somatic cells is rare, probably due to the fact that human chromosomes are not telocentric. In the case where whole-arm translocations are present, they are usually at the acrocentric chromosomes [38]. The distinct differences between mouse and human chromosomal structures led us to believe that finding the link between BubR1 acetylation deficiency and whole-arm translocation in human cancer would not be easy. However, we were aware that some hematologic malignancies have been shown to display complex karyotypes. Therefore, we analyzed the cytogenetics of patients with various hematopoietic malignancies from Seoul National University Hospital (SNUH). We found that 83 out of 1,837 patients displayed whole-arm translocation. Among these cases, multiple myeloma exhibited the highest frequency (11.6%,  $n = 334$ ), followed by myelodysplastic neoplasms (8%,  $n = 158$ ) (Table 2).

Taking this information into account, we searched for multiple myeloma cell lines that displayed whole-arm translocation to assess the association of BubR1 acetylation deficiency with whole-arm translocation in human malignancies. We found two multiple myeloma cell lines, KMS-12-BM [39] and SNU-1393-SC [40], for which the complete cytogenetics were available. For comparison purposes, we also included the multiple myeloma cell lines NCI-H929, which was negative for whole-arm translocation [41], and MM.1R, which lacked complete cytogenetic information [42], in our immunoprecipitation and western blot analyses (Table 3).

Cells were treated with nocodazole to induce mitotic arrest and were then subjected to immunoprecipitation using an anti-BubR1 antibody, followed by western blot using a monoclonal anti-acetyl-K250 antibody [8]. Our data supported that the whole-arm translocations may have been associated with BubR1 acetylation deficiency in these cells. The two cell lines with whole-arm translocation, KMS-12-BM and SNU-1393-SC, displayed a reduction in BubR1 acetylation, whereas NCI-H929 and MM.1R exhibited approximately 5- to 10-fold more K250 BubR1 acetylation (Fig. 6C, right, see numbers at bottom), reflecting intact BubR1 acetylation. The total BubR1 expression levels varied in the cell lysates of the cell lines, as determined by western

blot (Fig. 6C, left). However, the lysates were normalized prior to immunoprecipitation, as shown by western blot using the anti-BubR1 antibody (Fig. 6C, right). Altogether, these results indicated the possibility of an association between the loss of BubR1 acetylation and human cancers with complex chromosomal rearrangements, including whole-arm translocation.

## Discussion

Micronuclei, missense mutations, PMSCS, and various chromosomal rearrangements were hallmarks of tumors derived from the *K243R/+* mice, along with aneuploidy [11]. The combined chromosomal and genetic instability induced by loss of BubR1 acetylation in these tumors led us to explore the underlying molecular mechanism. To accomplish this, it was necessary to identify the chromosomal defects that were lost during development of the *K243R/+* mice, so we crossed the *K243R/+* mice with *p53-/-* mice to avoid apoptosis and obtain the *K243R/+;p53-/-* mice for further investigations. Because eight out of eleven primary tumors from the *K243R/+* mice displayed *p53* missense mutations [11], our breeding scheme was physiologically, although partially, supported.

As expected, tumor latency was accelerated to approximately 20 weeks in the *K243R/+;p53-/-* mice, similar to the *p53-/-* mice. However, there were several unexpected observations in these mice. First, the tumor spectrum changed. Tumors from the *K243R/+* mice were found in a wide variety of tissues, mostly of mesenchymal origin. In contrast, the tumor spectrum of the *K243R/+;p53-/-* mice resembled that of the *p53-/-* mice, except there was a decrease in thymic lymphomas and an increase in sarcomas (Fig. 1B). This may have been because rapidly proliferating tissues during the early stages after birth, including T cells in the thymus, were more susceptible to the accelerated tumorigenesis. The increased sarcomas may have been due to their mesenchymal origin, which was affected by the *K243R* allele.

We previously showed that *K243R/+* cells exhibited a high number of micronuclei containing damaged DNA [11]. Here, we provided evidence that these micronuclei, which resulted from the loss of BubR1 acetylation and subsequent chromosomal mis-segregation, contributed to genetic instability. It has been shown that the majority of micronuclei undergo defective nuclear envelope assembly and rupture, and disrupted micronuclei fail to recruit components necessary for genetic integrity, resulting in DNA damage [43,44]. The *K243R/+* and *K243R/+;p53-/-* MEFs displayed significantly increased DNA damage in



micronuclei compared with the *p53*<sup>−/−</sup> MEFs (Fig. 2E), indicating incomplete replication (Fig. 2F). If the DNA in micronuclei persist and incorporate into genome, marked increase in micronuclei in *K243R*/<sup>+</sup> would significantly contribute to the genetic instability. Notably, we showed that BubR1 acetylation deficiency resulted in the replication stress of nuclear DNA. Whether the replication stress is due to aneuploidy or due to the contribution from the micronuclei has not been fully elucidated. Yet, it is likely that the combination of aneuploidy and micronuclei cooperated to result in severe replication impediment in *K243R*/<sup>+</sup>; *p53*<sup>−/−</sup> cells, which grew faster than *K243R*/<sup>+</sup> cells. In this case, the absence of *p53* could have overcome the senescence or apoptosis invoked by the aneuploidy-induced replication stress.

We identified that the loss of BubR1 acetylation resulted in telomere fragility. The nature of telomeric repeats and the increase in aneuploidy may have been the reason for telomere replication stress in the *K243R*/<sup>+</sup> mice. However, *p53*<sup>−/−</sup> MEFs, which displayed a high degree of aneuploidy (Fig. 2A), exhibited significantly less replication stress at centromeres and telomeres (Fig. 3C,D), compared to the *K243R*/<sup>+</sup> MEFs. Therefore, there is a possibility that the telomere fragility observed in the *K243R*/<sup>+</sup> MEFs may be a more direct result of the loss of BubR1 acetylation than aneuploidy. Interestingly, a recent study has shown that the Bub1/Bub3 complex, components of the mitotic checkpoint that interact with BubR1, promotes telomere replication during S phase [45]. Therefore, defective BubR1 acetylation may have affected the integrity of the Bub3/Bub1 complex during telomere replication. Alternatively, mitotic infidelity may have affected replication integrity, which has been previously reported in yeast [46]. Indeed, the telomere fragility persisted through interphase in *K243R*/<sup>+</sup>; *p53*<sup>−/−</sup> MEFs (Fig. 3E,F).

Mechanisms of centromere establishment and specification are very different from those of telomeres [47,48]. Centromeres do not require specific nucleotide sequences and are epigenetically specified by the loading of centromere specification proteins. In contrast, telomeres consist of (TTAGGG)<sub>n</sub> repeats and are capped through the formation of telomere loops (T-loops). Unprotected telomeres are exposed to DNA damage response pathways, inducing recombination [49]. The whole-arm translocations occurring in the tumors from the *K243R*/<sup>+</sup>; *p53*<sup>−/−</sup> mice may be due to the precipitation of telomere fragility, resulting in telomere attrition and repair. Thus, deficiency of BubR1 acetylation, which mainly functions at the centromeric kinetochore, affected the integrity of telomeres at the chromosomal ends, and the telomere attrition and resultant end-end

fusions again affected the centromere specification, as the centromere in the fused chromosome appears to function. It would be interesting to see whether these Robertsonian-like chromosomes could be detected in germ cells of *K243R*/<sup>+</sup>; *p53*<sup>−/−</sup> mice and be inherited to the next generation. If so, loss of BubR1 acetylation may influence the meiotic drive.

Dicentric chromosomes resulting from end-to-end fusions may cause chromosome shattering and thus lead to chromothripsis and kataegis [26]. Due to complex inter- and intrachromosomal rearrangements, we were not able to detect chromothripsis and kataegis in the *K243R*/<sup>+</sup> or *K243R*/<sup>+</sup>; *p53*<sup>−/−</sup> tumors. Nevertheless, the possibility of chromothripsis and kataegis in the *K243R*/<sup>+</sup> cells remains. Notably, *BRCA2* deficiency, which is associated with BubR1 acetylation deficiency, is likely linked with kataegis [50].

In human malignancies [51], whole-arm translocations are found in acrocentric chromosomes, in which the centromere is located near one end of the chromosome [38]. Nonetheless, our findings suggest that defects in BubR1 acetylation may be associated with whole-arm translocations in a subset of human multiple myeloma (Fig. 6C).

An earnest question was whether BubR1 K250 mutation or acetylation deficiency occurred in human cancers. We found pathogenic mutations that display K250 acetylation deficiency in human cancers. L249F and A251P mutant BubR1 found from human cancers lacked the ability to acetylate K250 in mitosis, which are in complete agreement with the molecular mechanism how PCAF recognizes its target lysine.

It should be noted that *BRCA2*-deficient cancers exhibit defective BubR1 acetylation, as *BRCA2* serves as a scaffold for PCAF acetyltransferase and BubR1 binding in prometaphase. Hence, the absence of *BRCA2* results in deficiency of K250 acetylation of BubR1 without apparent mutation of BubR1 [10]. We showed previously that forced expression of an acetylation-mimetic form of BubR1 (K250Q) induces apoptosis in *BRCA2*-deficient cells [10]. Furthermore, *BRCA2*-deficient cells exhibit resistance to pan-HDAC inhibitors due to the lack of BubR1 acetylation, while they are sensitive to a specific type of epigenetic HDAC inhibitor [8]. It would be interesting to determine whether cancers with defective BubR1 acetylation respond similarly to K250Q expression or to a specific group of HDAC inhibitors.

Previously, we have seen that BubR1 levels are associated with poor prognosis for recurrence-free survival in ovarian cancer patients after surgery [52]. As shown here, assessment of BubR1 acetylation levels using monoclonal antibodies specific to acetylated BubR1 at

K250 may be clinically useful. Moreover, targeting the BubR1 acetylation pathway may be an effective treatment strategy for cancers with complex chromosomal rearrangements.

## Materials and methods

### Statistical analysis

The probability of tumor-free survival was estimated using the Kaplan–Meier method and analyzed by the log-rank test. Student's t-test was used for other statistical analyses, unless otherwise stated. Statistical data were analyzed using GRAPHPAD PRISM5 (GraphPad Software, Inc., San Diego, CA, USA).

### Cell culture, plasmids, and transfection

The multiple myeloma cell line, SNU-1393-SC, was previously established [40]. The NCI-H929, MM1R, and KMS-12-BM cell lines were obtained from either American Type Culture Collection (ATCC) (Manassas, VA, USA) or Deutsche Sammlung von Mikroorganismen und Zellkulturen (DSMZ) (Braunschweig, Germany). HEK293T cells and mouse tumor cells were cultured in Dulbecco's modified Eagle medium (DMEM), supplemented with 10% fetal bovine serum (Lonza, Basel, Switzerland). Various BubR1 mutants were generated by site-directed mutagenesis using pcDNA3.1-Myc-BubR1 as the template. PCAF (352–832 amino acids) was subcloned into the pCMV3xFLAG [7]. The BubR1 mutant constructs and pCMV3xFLAG-PCAF were transfected into HEK293T cells using Lipofectamine 2000 (Invitrogen, Carlsbad, CA, USA).

### Animal care and study approval

The previously generated *K243R/+* mice were used in this study [11]. The *K243R/+* mice were crossed with the *p53+/-* mice (B6. Cg-Trp53<sup>tm1Ty</sup>/J) several times to obtain the *K243R/+;p53-/-* mice. All mice used in this study were of a B6; 129 mixed background. Mice were housed in a specific pathogen-free facility. The Institutional Animal Care and Use Committee of Seoul National University (SNU-191007-4) approved the experimental animal protocols. We followed the guidelines and policies for the Care and Use of Laboratory Animals at Seoul National University. Karyotype analysis of hematologic malignancies from Seoul National University Hospital (SNUH) was approved by the SNUH Institutional Review Board (1103-004-353).

### Histopathology

Tissues were harvested from the following organs: thymus, lungs, liver, spleen, skin, spine, and lymph nodes. Tissues

were fixed in 4% formaldehyde, embedded in paraffin, and sectioned. The sections were deparaffinized in xylene, rehydrated in ethanol, and subjected to hematoxylin and eosin (H&E) staining. Two different pathologists made the disease diagnoses by analyzing the H&E-stained specimens (Logone Bio Convergence Research Foundation, Korea).

### Detection of somatic copy number alterations

Somatic copy number alterations (SCNAs) were identified using BIC-seq2 (version 0.6.3) [27]. The BIC-seq2 algorithm was composed of two main components. First, we normalized potential biases in the aligned sequencing reads data, based on the mouse reference genome (GRCm38), at the nucleotide level with a 1000-bp binning parameter. Second, SCNAs were detected based on Bayesian information criterion-based segmentation. We used three as the lambda parameter value, the main parameter for defining the smoothness of the SCNA profile.

### Detection of structural variations

The identification of chromosomal structural variations (SVs) was conducted using MEERKAT (version 0.189) [28]. Sequencing reads were aligned against the mouse reference genome (GRCm38) to identify soft-clipped and unmapped reads. These reads were remapped to identify discordant read pairs. After adjusting nonuniquely mapped reads, we paired clusters to call multiple events. Candidates of breakpoint regions were predicted by supporting reads, and precise breakpoints were identified by local alignments. Somatic events were obtained by further processes filtering out germline and low confidence calls.

### Detection of somatic single-nucleotide variations and short indels

We used MuTect2, included in the GENOME ANALYSIS TOOLKIT (version 3.5), with default parameters to detect somatic single-nucleotide variations (SNVs) and short indels [53]. MuTect2 applied a Bayesian classifier to identify somatic SNVs and short indels with low allele fractions, followed by careful filtering processes that allowed high specificity of each mutation.

### Metaphase spreads and fluorescence *in situ* hybridization

Metaphase chromosome spreads and fluorescence *in situ* hybridization (FISH) were performed, as previously described [54]. Images were acquired with a microscope (DeltaVision; Applied Precision, Issaquah, WA, USA) equipped with a 60× objective lens (Olympus, Tokyo, Japan). The images were then obtained with optical

sections at a 0.2- $\mu\text{m}$  distance in the z-axis. Each section was deconvoluted and projected using the softWoRx software (Applied Precision).

### Antibodies and immunoprecipitation, western blot, and immunofluorescence assays

The following antibodies were used in this study: antiphospho-histone H2A.X (Ser 139; Millipore, Burlington, MA, USA); antihuman anticentromere antibodies (CREST; Antibodies Incorporated, Davis, CA, USA); anti-c-Myc (9E10) (sc-40; Santa Cruz Biotechnology, Santa Cruz, CA, USA); antihuman BubR1 (612503; BD Biosciences, San Jose, CA, USA); anti-GAPDH (AbC-1001; AbClon, Seoul, South Korea); anti-FLAG (M2) (F1804; Sigma-Aldrich, St. Louis, MO, USA); anti-Lamin A/C (sc-7292; Santa Cruz Biotechnology); rat monoclonal anti-BrdU (BU1/75 (ICR1); AbD Serotec, Kidlington, UK); and anti-BrdU (B44; BD Bioscience). A home-made rabbit monoclonal antibody against acetylated BubR1 at K250 was also used [8]. For mitotic arrest, HEK293T or multiple myeloma cells were treated with nocodazole for 18 h with 200  $\text{ng}\cdot\text{mL}^{-1}$  nocodazole (Sigma-Aldrich). The cells were then lysed and subjected to immunoprecipitation, followed by western blot, as previously described [7,8]. Immunofluorescence was performed according to a previously published protocol with slight modifications [7].

### Spectral karyotyping assay

Tumor cells from the *K243R/+; p53-/-* mice were treated with 5  $\mu\text{g}\cdot\text{mL}^{-1}$  colcemid for 2 h, followed by fixation. The spectral karyotyping assay was performed at the Molecular Cytogenetics Core at the University of Texas M.D. Anderson Cancer Center (Houston, TX, USA).

### EdU incorporation assay

Mouse embryonic fibroblasts were labeled with 10  $\mu\text{M}$  EdU for 12 h at 37 °C and then fixed with 4% paraformaldehyde. Edu incorporation was visualized by incubation in [3 + 2] cycloaddition reaction buffer (2 mM  $\text{CuSO}_4$ , 8  $\mu\text{M}$  sulfo-cyanine5 azide, and 20  $\text{mg}\cdot\text{mL}^{-1}$  ascorbic acid). Fixed cells were then processed for immunofluorescence.

### DNA fiber assay

Mouse embryonic fibroblasts were labeled with 25  $\mu\text{M}$  IdU for 20 min at 37 °C and then labeled with 250  $\mu\text{M}$  CldU for 40 min at 37 °C. IdU/CldU-labeled MEFs were trypsinized, washed, and resuspended in culture medium. The suspension was mixed with nonlabeled MEFs and fixed in methanol/acetic acid (3 : 1) fixative. Fixed cells were mounted onto clean slides and dried for 2 min at room

temperature. The slides were incubated in a Coplin jar filled with lysis buffer (0.5% SDS, 50 mM EDTA, and 200 mM Tris/HCl [pH.7.0]) for 15 min at 37 °C and then in a humidified chamber for 10 min at 37 °C to allow DNA fiber extension. The extended DNA was fixed with fixative, dried, and incubated in denaturation buffer (2.5  $\text{mol}\cdot\text{L}^{-1}$  HCl) for 75 min at room temperature. Incorporated IdU/CldU was detected by immunofluorescence assay.

### Acknowledgements

This work was supported by Tissue Regeneration Research (2016M3A9B4918405) and Post-Genome Research (2017M3C9A5030991, 2017M3C9A5031002, and 2017M3C9A5031004) from the Korean Research Foundation. We thank A. H. Yoo for critical reading of the manuscript. We are grateful to all members of the Lee laboratory for the helpful discussions throughout the study. The presented results are partially based on data generated by the TCGA Research Network (<https://www.cancer.gov/tcga>).

### Conflict of interest

The authors declare no conflict of interest.

### Author contributions

HL initiated and led the project and wrote the manuscript; JP and SY conceived, designed, and performed experiments; JP, SP, HK, SC, and JL performed experiments for chromosome analyses; JH and SL performed genomic analyses; YK collected patient data and was responsible for IRB approval.

### Peer Review

The peer review history for this article is available at <https://publons.com/publon/10.1111/febs.15912>.

### References

- 1 Weaver BA, Silk AD, Montagna C, Verdier-Pinard P & Cleveland DW (2007) Aneuploidy acts both oncogenically and as a tumor suppressor. *Cancer Cell* **11**, 25–36.
- 2 Varetto G, Guida C, Santaguida S, Chirolì E & Musacchio A (2011) Homeostatic control of mitotic arrest. *Mol Cell* **44**, 710–720.
- 3 Di Fiore B, Wurzenberger C, Davey NE & Pines J (2016) The mitotic checkpoint complex requires an evolutionary conserved cassette to bind and inhibit active APC/C. *Mol Cell* **64**, 1144–1153.

- 4 Alfieri C, Chang L, Zhang Z, Yang J, Maslen S, Skehel M & Barford D (2016) Molecular basis of APC/C regulation by the spindle assembly checkpoint. *Nature* **536**, 431–436.
- 5 Wang Q, Liu T, Fang Y, Xie S, Huang X, Mahmood R, Ramaswamy G, Sakamoto KM, Darzynkiewicz Z, Xu M *et al.* (2004) BUBR1 deficiency results in abnormal megakaryopoiesis. *Blood* **103**, 1278–1285.
- 6 Baker DJ, Jeganathan KB, Cameron JD, Thompson M, Juneja S, Kopecka A, Kumar R, Jenkins RB, de Groen PC, Roche P *et al.* (2004) BubR1 insufficiency causes early onset of aging-associated phenotypes and infertility in mice. *Nat Genet* **36**, 744–749.
- 7 Choi E, Choe H, Min J, Choi JY, Kim J & Lee H (2009) BubR1 acetylation at prometaphase is required for modulating APC/C activity and timing of mitosis. *EMBO J* **28**, 2077–2089.
- 8 Park I, Kwon MS, Paik S, Kim H, Lee HO, Choi E & Lee H (2017) HDAC2/3 binding and deacetylation of BubR1 initiates spindle assembly checkpoint silencing. *FEBS J* **284**, 4035–4050.
- 9 Di Fiore B, Davey NE, Hagting A, Izawa D, Mansfeld J, Gibson TJ & Pines J (2015) The ABBA motif binds APC/C activators and is shared by APC/C substrates and regulators. *Dev Cell* **32**, 358–372.
- 10 Choi E, Park P-G, Lee H-O, Lee Y-K, Kang GH, Lee JW, Han W, Lee HC, Noh D-Y & Lekomtsev S (2012) BRCA2 fine-tunes the spindle assembly checkpoint through reinforcement of BubR1 acetylation. *Dev Cell* **22**, 295–308.
- 11 Park I, Lee HO, Choi E, Lee YK, Kwon MS, Min J, Park PG, Lee S, Kong YY, Gong G *et al.* (2013) Loss of BubR1 acetylation causes defects in spindle assembly checkpoint signaling and promotes tumor formation. *J Cell Biol* **202**, 295–309.
- 12 Crasta K, Ganem NJ, Dagher R, Lantermann AB, Ivanova EV, Pan Y, Nezi L, Protopopov A, Chowdhury D & Pellman D (2012) DNA breaks and chromosome pulverization from errors in mitosis. *Nature* **482**, 53–58.
- 13 Zhang CZ, Spektor A, Cornils H, Francis JM, Jackson EK, Liu S, Meyerson M & Pellman D (2015) Chromothripsis from DNA damage in micronuclei. *Nature* **522**, 179–184.
- 14 Stephens PJ, Greenman CD, Fu B, Yang F, Bignell GR, Mudie LJ, Pleasance ED, Lau KW, Beare D, Stebbings LA *et al.* (2011) Massive genomic rearrangement acquired in a single catastrophic event during cancer development. *Cell* **144**, 27–40.
- 15 Lee YK, Park I & Lee H (2014) Partial hepatectomy in acetylation-deficient BubR1 mice corroborates that chromosome missegregation initiates tumorigenesis. *Endocrinol Metab (Seoul)* **29**, 561–566.
- 16 Santaguida S & Amon A (2015) Short- and long-term effects of chromosome mis-segregation and aneuploidy. *Nat Rev Mol Cell Biol* **16**, 473–485.
- 17 Sheltzer JM, Ko JH, Replogle JM, Habibe Burgos NC, Chung ES, Meehl CM, Sayles NM, Passerini V, Storchova Z & Amon A (2017) Single-chromosome gains commonly function as tumor suppressors. *Cancer Cell* **31**, 240–255.
- 18 Jacks T, Remington L, Williams BO, Schmitt EM, Halachmi S, Bronson RT & Weinberg RA (1994) Tumor spectrum analysis in p53-mutant mice. *Curr Biol* **4**, 1–7.
- 19 Donehower LA, Harvey M, Slagle BL, McArthur MJ, Montgomery CA Jr, Butel JS & Bradley A (1992) Mice deficient for p53 are developmentally normal but susceptible to spontaneous tumours. *Nature* **356**, 215–221.
- 20 Aylon Y & Oren M (2011) p53: guardian of ploidy. *Mol Oncol* **5**, 315–323.
- 21 Merrick CJ, Jackson D & Diffley JF (2004) Visualization of altered replication dynamics after DNA damage in human cells. *J Biol Chem* **279**, 20067–20075.
- 22 Frum RA, Khondker ZS & Kaufman DG (2009) Temporal differences in DNA replication during the S phase using single fiber analysis of normal human fibroblasts and glioblastoma T98G cells. *Cell Cycle* **8**, 3133–3148.
- 23 Zeman MK & Cimprich KA (2014) Causes and consequences of replication stress. *Nat Cell Biol* **16**, 2–9.
- 24 Forment JV, Kaidi A & Jackson SP (2012) Chromothripsis and cancer: causes and consequences of chromosome shattering. *Nat Rev Cancer* **12**, 663–670.
- 25 Rausch T, Jones DT, Zapatka M, Stutz AM, Zichner T, Weischenfeldt J, Jager N, Remke M, Shih D, Northcott PA *et al.* (2012) Genome sequencing of pediatric medulloblastoma links catastrophic DNA rearrangements with TP53 mutations. *Cell* **148**, 59–71.
- 26 Maciejowski J, Li Y, Bosco N, Campbell PJ & de Lange T (2015) Chromothripsis and kataegis induced by telomere crisis. *Cell* **163**, 1641–1654.
- 27 Xi R, Lee S, Xia Y, Kim TM & Park PJ (2016) Copy number analysis of whole-genome data using BIC-seq2 and its application to detection of cancer susceptibility variants. *Nucleic Acids Res* **44**, 6274–6286.
- 28 Yang L, Luquette LJ, Gehlenborg N, Xi R, Haseley PS, Hsieh CH, Zhang C, Ren X, Protopopov A, Chin L *et al.* (2013) Diverse mechanisms of somatic structural variations in human cancer genomes. *Cell* **153**, 919–929.
- 29 Korbel JO & Campbell PJ (2013) Criteria for inference of chromothripsis in cancer genomes. *Cell* **152**, 1226–1236.
- 30 Bonilla X, Parmentier L, King B, Bezrukov F, Kaya G, Zoete V, Seplyarskiy VB, Sharpe HJ, McKee T, Letourneau A *et al.* (2016) Genomic analysis identifies new drivers and progression pathways in skin basal cell carcinoma. *Nat Genet* **48**, 398–406.

- 31 Hodis E, Watson IR, Kryukov GV, Arold ST, Imielinski M, Theurillat JP, Nickerson E, Auclair D, Li L, Place C *et al.* (2012) A landscape of driver mutations in melanoma. *Cell* **150**, 251–263.
- 32 Hugo W, Zaretsky JM, Sun L, Song C, Moreno BH, Hu-Lieskovan S, Berent-Maoz B, Pang J, Chmielowski B, Cherry G *et al.* (2016) Genomic and transcriptomic features of response to anti-PD-1 therapy in metastatic melanoma. *Cell* **165**, 35–44.
- 33 Krauthammer M, Kong Y, Ha BH, Evans P, Bacchicocchi A, McCusker JP, Cheng E, Davis MJ, Goh G, Choi M *et al.* (2012) Exome sequencing identifies recurrent somatic RAC1 mutations in melanoma. *Nat Genet* **44**, 1006–1014.
- 34 Shern JF, Chen L, Chmielecki J, Wei JS, Patidar R, Rosenberg M, Ambrogio L, Auclair D, Wang J, Song YK *et al.* (2014) Comprehensive genomic analysis of rhabdomyosarcoma reveals a landscape of alterations affecting a common genetic axis in fusion-positive and fusion-negative tumors. *Cancer Discov* **4**, 216–231.
- 35 Cerami E, Gao J, Dogrusoz U, Gross BE, Sumer SO, Aksoy BA, Jacobsen A, Byrne CJ, Heuer ML, Larsson E *et al.* (2012) The cBio cancer genomics portal: an open platform for exploring multidimensional cancer genomics data. *Cancer Discov* **2**, 401–404.
- 36 Gao J, Aksoy BA, Dogrusoz U, Dresdner G, Gross B, Sumer SO, Sun Y, Jacobsen A, Sinha R, Larsson E *et al.* (2013) Integrative analysis of complex cancer genomics and clinical profiles using the cBioPortal. *Sci Signal* **6**, pii.
- 37 Mujtaba S, Zeng L & Zhou MM (2007) Structure and acetyl-lysine recognition of the bromodomain. *Oncogene* **26**, 5521–5527.
- 38 Hecht F, Morgan R & Hecht BK (1988) Robertsonian chromosome recombinants are rare in cancer. *Cancer Genet Cytogenet* **35**, 79–81.
- 39 Ohtsuki T, Yawata Y, Wada H, Sugihara T, Mori M & Namba M (1989) Two human myeloma cell lines, amylase-producing KMS-12-PE and amylase-non-producing KMS-12-BM, were established from a patient, having the same chromosome marker, t(11;14)(q13;q32). *Br J Haematol* **73**, 199–204.
- 40 Koh Y, Jung WJ, Ahn KS & Yoon SS (2014) Establishment of cell lines from both myeloma bone marrow and plasmacytoma: SNU\_MM1393\_BM and SNU\_MM1393\_SC from a single patient. *Biomed Res Int* **2014**, 510408.
- 41 Gazdar AF, Oie HK, Kirsch IR & Hollis GF (1986) Establishment and characterization of a human plasma cell myeloma culture having a rearranged cellular myc proto-oncogene. *Blood* **67**, 1542–1549.
- 42 Goldman-Leikin RE, Salwen HR, Herst CV, Variakojis D, Bian ML, Le Beau MM, Selvanayagan P, Marder R, Anderson R, Weitzman S *et al.* (1989) Characterization of a novel myeloma cell line, MM.1. *J Lab Clin Med* **113**, 335–345.
- 43 Terradas M, Martin M, Hernandez L, Tusell L & Genesca A (2012) Nuclear envelope defects impede a proper response to micronuclear DNA lesions. *Mutat Res-Fund Mol M* **729**, 35–40.
- 44 Hatch EM, Fischer AH, Deerinck TJ & Hetzer MW (2013) Catastrophic nuclear envelope collapse in cancer cell micronuclei. *Cell* **154**, 47–60.
- 45 Li F, Kim H, Ji Z, Zhang T, Chen B, Ge Y, Hu Y, Feng X, Han X, Xu H *et al.* (2018) The BUB3-BUB1 complex promotes telomere DNA replication. *Mol Cell* **70**, 395–407 e4.
- 46 Magiera MM, Gueydon E & Schwob E (2014) DNA replication and spindle checkpoints cooperate during S phase to delay mitosis and preserve genome integrity. *J Cell Biol* **204**, 165–175.
- 47 Gascoigne KE, Takeuchi K, Suzuki A, Hori T, Fukagawa T & Cheeseman IM (2011) Induced ectopic kinetochore assembly bypasses the requirement for CENP-A nucleosomes. *Cell* **145**, 410–422.
- 48 Hori T, Amano M, Suzuki A, Backer CB, Welburn JP, Dong Y, McEwen BF, Shang WH, Suzuki E, Okawa K *et al.* (2008) CCAN makes multiple contacts with centromeric DNA to provide distinct pathways to the outer kinetochore. *Cell* **135**, 1039–1052.
- 49 De Lange T (2005) Telomere-related genome instability in cancer. *Cold Spring Harb Symp Quant Biol* **70**, 197–204.
- 50 Alexandrov LB, Nik-Zainal S, Wedge DC, Aparicio SA, Behjati S, Biankin AV, Bignell GR, Bolli N, Borg A, Borresen-Dale AL *et al.* (2013) Signatures of mutational processes in human cancer. *Nature* **500**, 415–421.
- 51 Adeyinka A, Wei S & Sanchez J (2007) Loss of 17p is a major consequence of whole-arm chromosome translocations in hematologic malignancies. *Cancer Genet Cytogenet* **173**, 136–143.
- 52 Lee YK, Choi E, Kim MA, Park PG, Park NH & Lee H (2009) BubR1 as a prognostic marker for recurrence-free survival rates in epithelial ovarian cancers. *Br J Cancer* **101**, 504–510.
- 53 Cibulskis K, Lawrence MS, Carter SL, Sivachenko A, Jaffe D, Sougnez C, Gabriel S, Meyerson M, Lander ES & Getz G (2013) Sensitive detection of somatic point mutations in impure and heterogeneous cancer samples. *Nat Biotechnol* **31**, 213–219.
- 54 Min J, Choi ES, Hwang K, Kim J, Sampath S, Venkitaraman AR & Lee H (2012) The breast cancer susceptibility gene BRCA2 is required for the maintenance of telomere homeostasis. *J Biol Chem* **287**, 5091–5101.